Effects of Administration Route, Dietary Condition, and Blood Glucose Level on Kinetics and Uptake of ^{18}F-FDG in Mice

Koon-Pong Wong[1], Wei Sha[1], Xiaoli Zhang[1], and Sung-Cheng Huang[1,2]

[1]Department of Molecular and Medical Pharmacology, David Geffen School of Medicine at UCLA, Los Angeles, California; and [2]Department of Biomathematics, David Geffen School of Medicine at UCLA, Los Angeles, California

The effects of dietary condition and blood glucose level on the kinetics and uptake of ^{18}F-FDG in mice were systematically investigated using intraperitoneal and tail-vein injection. **Methods:** Dynamic PET was performed for 60 min on 23 isoflurane-anesthetized male C57BL/6 mice after intravenous (n = 11) or intraperitoneal (n = 12) injection of ^{18}F-FDG. Five and 6 mice in the intravenous and intraperitoneal groups, respectively, were kept fasting overnight (18 ± 2 h), and the others were fed ad libitum. Serial blood samples were collected from the femoral artery to measure ^{18}F-FDG and glucose concentrations. Image data were reconstructed using filtered backprojection with CT-based attenuation correction. The standardized uptake value (SUV) was estimated from the 45- to 60-min image. The metabolic rate of glucose (MRGlu) and ^{18}F-FDG uptake constant (K_i) were derived by Patlak graphical analysis. **Results:** In the brain, SUV and K_i were significantly higher in fasting mice with intraperitoneal injection, but MRGlu did not differ significantly under different dietary states and administration routes. Cerebral K_i was inversely related to elevated blood glucose levels, irrespective of administration route or dietary state. In myocardium, SUV, K_i, and MRGlu were significantly lower in fasting than in nonfasting mice for both routes of injection. Myocardial SUV and K_i were strongly dependent on the dietary state, and K_i did not correlate with the blood glucose level. Similar results were obtained for skeletal muscle, although the differences were not as pronounced. **Conclusion:** Intraperitoneal injection is a valid alternative route, providing pharmacokinetic data equivalent to data from tail-vein injection for small-animal ^{18}F-FDG PET. Cerebral K_i varies inversely with blood glucose level, but the measured cerebral MRGlu does not correlate with blood glucose level or dietary condition. Conversely, the K_i values of the myocardium and skeletal muscle are strongly dependent on dietary condition but not on blood glucose level. In tissue in which ^{18}F-FDG uptake declines with increasing blood glucose, correction for blood glucose level will make SUV a more robust outcome measure of MRGlu.

Key Words: blood glucose; dietary condition; ^{18}F-FDG; glucose metabolism; intraperitoneal injection

J Nucl Med 2011; 52:800–807
DOI: 10.2967/jnumed.110.085092

Small-animal imaging of labeled compounds using PET has been increasingly applied in murine models of human diseases. Specifically, the glucose analog ^{18}F-FDG, which has been used for the in vivo measurement of local glucose utilization in humans with PET (*1*), is playing a pivotal role in mouse models to study tissue responses due to various drug or treatment interventions and diseases, including cancers. As an extension of the 2-^{14}C-deoxy-D-glucose autoradiographic method (*2*), the ^{18}F-FDG PET technique determines glucose utilization in a local tissue according to an operational equation and compartmental model fitting (*1*) or a semiquantitative index such as standardized uptake value (SUV), which normalizes tissue ^{18}F-FDG uptake by injected dose per body weight (*3,4*). This method usually uses an intravenous injection of the labeled glucose analog and requires assays of plasma glucose level and the time course of radioactivity concentrations in plasma through peripheral blood sampling. In particular, intravenous injection requires proper animal-handling techniques (*5*), thereby imposing several technical challenges on small-animal PET. Intraperitoneal injection is much more convenient and practical in rodents (*6*). For mouse ^{18}F-FDG PET studies, intraperitoneal injection has been shown to provide biodistribution data comparable to those obtained using intravenous injection within 60 min after injection (*7*). However, the effects of the injection route on ^{18}F-FDG kinetics in various tissues have not been fully studied.

Because both ^{18}F-FDG and glucose enter the cells using the same glucose transporters, variations of plasma glucose level and dietary changes can affect ^{18}F-FDG uptake in tissues. Therefore, understanding the impact of dietary condition and blood glucose level on ^{18}F-FDG uptake and ^{18}F-FDG kinetics in various tissues may improve the reliability of using ^{18}F-FDG PET to measure local tissue function and glucose metabolism. Earlier results from in vitro and in vivo studies have indicated that ^{18}F-FDG uptake in

Received Nov. 8, 2010; revision accepted Jan. 12, 2011.
For correspondence or reprints contact: Koon-Pong Wong, Department of Molecular and Medical Pharmacology, David Geffen School of Medicine at UCLA, Room B2-085E CHS, 10833 Le Conte Ave., Los Angeles, CA 90095.
E-mail: kpwong@ucla.edu
Guest Editor: Sanjiv Gambhir, Stanford University

cancer cells lessens with increasing blood glucose level (*8,9*). A significant reduction of tumor ^{18}F-FDG uptake during the glucose-loaded state, compared with the fasting state, has also been reported in clinical PET studies (*10,11*). Similarly, cerebral ^{18}F-FDG uptake has been shown to be decreased when blood glucose level is elevated (*9,12*), whereas myocardial ^{18}F-FDG uptake is diminished by fasting (*12,13*). However, a more systematic investigation that considers these preclinical and clinical factors is still needed to help increase the robustness of ^{18}F-FDG uptake and kinetics as a reliable outcome measure. The aims of this study were, first, to investigate the impact of dietary condition (nonfasting vs. fasting) and altered blood glucose level on ^{18}F-FDG kinetics, uptake profiles, and kinetic or physiologic parameters in normal tissues of intact mice using dynamic small-animal PET and, second, to evaluate the feasibility of using intraperitoneal ^{18}F-FDG injection as an alternative to tail-vein injection to study glucose metabolism in mice.

MATERIALS AND METHODS

Animal Preparations

All animal experiments were performed in accordance with institutional guidelines and a protocol approved by the Animal Research Committee of the University of California, Los Angeles. Twenty-three 6- to 18-wk-old male C57BL/6 mice (23.8 ± 3.1 g) were studied. Twelve (6 for intravenous injection studies and 6 for intraperitoneal injection studies) were fed ad libitum, and the rest (5 for intravenous injection studies and 6 for intraperitoneal injection studies) were kept fasting overnight (18 ± 2 h) but with free access to water. The animals were anesthetized with inhalant anesthesia (1.5%–2% isoflurane in 100% oxygen), and the left femoral artery was cannulated with a surgically inserted polyethylene catheter (Intramedic polyethylene tubing [PE 10]; Clay Adams) filled with heparinized saline. The body temperature of the mice was maintained at 36°C by a thermostat-controlled heating pad throughout the aseptic surgery for implanting the catheter. For intravenous injection studies, a 28.5-gauge needle connected to a 3- to 5-cm-long PE 20 catheter was inserted into the lateral tail vein for ^{18}F-FDG administration.

Small-Animal Imaging

Small-animal PET was performed on a microPET Focus 220 scanner (Concorde Microsystems, LLC). Each animal was placed prone inside an imaging chamber (*14*) specifically designed for small-animal PET and CT to allow for regulated temperature control and anesthesia delivery. List-mode PET data were acquired for 60 min immediately after ^{18}F-FDG was injected manually via the tail-vein catheter for intravenous injection studies (14.2 ± 3.8 MBq; ~60 μL) or into the peritoneal cavity for intraperitoneal injection studies (10.5 ± 0.8 MBq; ~50–100 μL). After the PET scan was completed, a 10-min CT scan was acquired with a small-animal CT scanner (MicroCAT II; ImTek Inc.).

Blood Sampling

Serial blood samples (~10–15 μL each) were collected with heparinized microhematocrit tubes (Fisherbrand; Fisher HealthCare) from the left femoral artery via the surgically inserted catheter. For intravenous injection studies, blood sampling took place at approximately 3, 5, 8, 25, 40, 60, 90, and 120 s and at 5, 10, 15, 30, 45, and 60 min. For intraperitoneal injection studies, blood sampling took place at 5, 10, 15, 20, 40, and 60 min. Arterial blood glucose levels were measured using a blood glucose meter (Ascensia Contour; Bayer HealthCare LLC) during the imaging experiment. With the exception of the first few samples in intravenous injection studies, when blood sampling needed to be performed rapidly, the catheter line was flushed with saline (~5–10 μL) after each timed sample and blood glucose measurement to clear the dead space and avoid excessive blood loss. Plasma samples were separated from whole-blood samples by centrifuging the microhematocrit tubes. Hematocrit was measured as the ratio of the length of the microhematocrit tube occupied by the red blood cells to that of the whole-blood sample. The whole-blood and plasma samples were pipetted to preweighed test tubes, weighed, and counted in a γ-counter (Wizard 3″; PerkinElmer Life Sciences).

Image Reconstruction

The list-mode PET data were binned to a framing protocol of 1 × 3 s, 10 × 0.5 s, 1 × 2 s, 1 × 4 s, 6 × 5 s, 1 × 10 s, 2 × 30 s, 2 × 120 s, 1 × 180 s, 2 × 600 s, and 2 × 900 s for intravenous injection studies. For intraperitoneal injection studies, the list-mode PET data were binned to a framing protocol of 12 × 5 min. The PET data were corrected for radioactive decay, random coincidences, and dead-time losses and were reconstructed using Fourier rebinning and a 2-dimensional filtered backprojection algorithm with a ramp filter cut off at the Nyquist frequency and a zoom factor of 4.74, resulting in a voxel size of 0.4 × 0.4 × 0.8 mm^3. The small-animal PET and CT images were coregistered using a published method (*15*), which is implemented in-house and has been performed routinely at our preclinical imaging center. The small-animal CT images were also used for attenuation correction of the PET data (*15*).

Image Analysis

Images were analyzed using AMIDE (http://amide.sourceforge.net/). Three-dimensional ellipsoid regions of interest (ROIs) were manually drawn over the brain, myocardium, skeletal muscle of the forelegs, left ventricle, liver, and renal cortex on the fused PET/CT images, which provided anatomic references for ROI placement. For the urinary bladder, ROIs that covered the entire bladder were drawn frame by frame as detailed elsewhere (*16*). ROIs were applied to each time frame of the PET images, and the average radioactivity concentration was computed to obtain the tissue time–activity curves. The total accumulated activity curve of the urinary bladder was calculated as the total activity within the ROIs defined frame by frame (*16*). Because uptake in the tissues was relatively homogeneous within the ROIs and the background radioactivity was low, background subtraction and partial-volume correction were not performed.

Equilibration of ^{18}F-FDG Between Plasma and Whole Blood

A time-dependent plasma–to–whole-blood ^{18}F-FDG equilibrium ratio, $R_{RB}(t)$, was determined between ^{18}F-FDG concentrations in plasma and whole blood for each study:

$$R_{PB}(t) = Ae^{-\beta t} + \rho, \qquad \text{Eq. 1}$$

where A (unitless), β (min^{-1}), and ρ (unitless) were estimated by nonlinear least-squares fitting to ^{18}F-FDG concentration ratios between plasma and whole-blood samples collected at different times t (min) throughout the PET acquisition.

Plasma Input Function

For intravenous injection studies, the complete time courses for the whole-blood and plasma input function had a better temporal resolution around the peak composed of the early-time left ventricle data ($t < 1$ min), with corrections for delay, dispersion, partial-volume effects (*17*), and red blood cell uptake (for plasma input function), and the serial femoral whole-blood and plasma sample measurements ($t \geq 1$ min). Details of the method are described in the Supplemental Appendix (supplemental materials are available online only at http://jnm.snmjournals.org). For intraperitoneal injection studies, manually drawn samples were used directly to form the whole-blood time–activity curve and plasma input function.

Kinetic Analysis

Both PET image data and blood data were converted to absolute radioactivity concentration (MBq/mL) with the cross-calibration factor derived from routine cylinder phantom experiments. The ^{18}F-FDG uptake constant (K_i) was estimated by Patlak graphical analysis (*18*) using plasma input function and time–activity data from 15–60 min and 30–60 min for intravenous and intraperitoneal injection studies, respectively. The early-time tissue data were not used because an equilibration time (t^*) is needed in establishing a steady-state condition when the Patlak plot becomes linear (*18*). The metabolic rate of glucose (MRGlu) was calculated as $MRGlu = K_iC_{glu}/LC$ (*1,2*), where C_{glu} is the mean plasma glucose concentration during the 60-min PET scan and LC is the lumped constant, which is assumed to be 0.6 for the brain (*19*) and 1.0 for myocardium and skeletal muscle. Time–activity data were also quantified using SUV (*3,4*):

$$SUV = \frac{\text{radioactivity concentration in region of interest (MBq/mL)}}{\text{injected dose (MBq)/weight of animal (g)}}. \quad \text{Eq. 2}$$

The small-animal PET and CT image files, blood sample data, and other experimental information for all studies discussed here are available online at the UCLA Mouse Quantitation Program Web site (http://dragon.nuc.ucla.edu/mqp/index.html).

Data Analysis

Results are presented as mean ± SD. Statistical analyses were performed using SAS, version 9.2 (SAS Institute Inc.), for Windows (Microsoft) and Prism, version 4.03 (GraphPad Software Inc.). Area under the curve of plasma input function (SUV × min) was calculated from 0 to 60 min by the trapezoidal rule. Plasma clearance rate (min^{-1}) was determined by a 1-exponential fit to the plasma samples taken after 30 min after injection of ^{18}F-FDG. Differences in physiologic parameters among the experimental groups of different administration routes and dietary conditions were compared by 2-way ANOVA with the Bonferroni post hoc test and by the Mann–Whitney *U* test whenever appropriate. Regression analysis was performed on tissue uptake (SUV), K_i, and MRGlu in the brain, myocardium, and skeletal muscle to investigate their relationships with blood glucose level, dietary state, plasma area under the curve, plasma clearance rate, and total radioactivity in the urinary bladder. A *P* value of less than 0.05 was considered statistically significant.

RESULTS

Physiologic Variables

At the beginning of the imaging experiments, mean blood glucose level was significantly higher in nonfasting than in fasting animals (11.0 ± 3.6 vs. 8.1 ± 2.9 mmol/L, $P = 0.028$). A modest increase in blood glucose level was observed in nonfasting and fasting animals (13.8 ± 4.1 vs. 10.7 ± 4.3 mmol/L, $P = 0.03$) after 60 min of imaging. Hematocrit was 0.45 ± 0.03 but decreased linearly (because of blood withdrawals and saline flushing) at a rate of $-0.00097 \pm 0.00034\ min^{-1}$ and $-0.00080 \pm 0.00048\ min^{-1}$ in animals receiving intravenous and intraperitoneal injection, respectively.

Equilibrations of ^{18}F-FDG Between Plasma and Whole Blood

Parameter estimates of the time-dependent equilibrium ratio between ^{18}F-FDG concentrations in plasma and whole blood obtained from different routes and dietary states are summarized in Supplemental Table 1. There was no significant main effect of administration route ($F(1,19) = 0.59$, $P = 0.45$) or of dietary state ($F(1,19) = 0.41$, $P = 0.53$) on the equilibrium ratio (ρ) of ^{18}F-FDG concentration between plasma and whole blood. The average value of ρ was 1.11 ± 0.08. The Bonferroni post hoc test indicated that $R_{PB}(t)$ reached equilibrium significantly more quickly with intravenous injection under the fasting condition ($P < 0.05$).

Delay, Dispersion, and Partial-Volume Corrections for Input Function

An example of a blood time–activity curve corrected for partial volume, delay, and dispersion in an intravenous injection study is shown in Supplemental Figure 1. No such correction was needed for intraperitoneal injection studies. As anticipated, the blood time–activity curve obtained from the left ventricular chamber preceded the blood samples drawn manually from the femoral artery because of delay and dispersion. There were no significant differences in delay or dispersion constants between nonfasting and fasting animals, and their estimates from the 2 groups were therefore pooled. The mean delay and dispersion constants between the left ventricle and the femoral artery catheter were 3.54 ± 1.81 s and 2.39 ± 1.32 s, respectively. The average recovery coefficient was 0.83 ± 0.10.

Plasma Input Function

Plasma time–activity curves obtained from intravenous and intraperitoneal injection studies are illustrated in Figure 1. Although the shape of the time–activity curves differed between intravenous and intraperitoneal injection studies, the radioactivity concentrations were comparable toward the end of the imaging experiment (Fig. 1A). Moreover, administration route ($F(1,19) = 0.10$, $P = 0.531$) and dietary state ($F(1,19) = 0.78$, $P = 0.388$) had no significant effect on area under the plasma curve.

For intravenous injection studies, plasma ^{18}F-FDG concentrations peaked within 10 s (Fig. 1A). No significant difference in ^{18}F-FDG plasma clearance rate was observed between nonfasting ($0.015 \pm 0.009\ min^{-1}$) and fasting ($0.018 \pm 0.0038\ min^{-1}$) animals, although the area under the plasma curve for the fasting state tended to be slightly

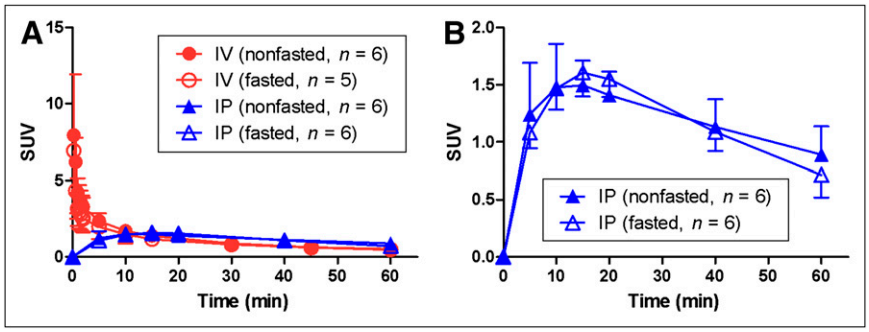

FIGURE 1. (A) Plasma time–activity curves obtained from nonfasting and fasting animals after intravenous (IV) or intraperitoneal (IP) injection of ^{18}F-FDG. (B) Plasma time–activity curves obtained only from intraperitoneally injected animals. Error bars represent 1 SD.

lower than that for the nonfasting state (62.6 ± 20.1 vs. 73.1 ± 22.6 SUV × min, $P = 0.214$).

The plasma input functions obtained with intraperitoneal injection had a much lower and broader peak than those obtained with intravenous injection (Fig. 1A). As shown in Figure 1B, plasma input function peaked slightly higher and later (at ~15 min) in fasting than in nonfasting animals (within 10–15 min). Dietary state had a significant effect on the ^{18}F-FDG plasma clearance rate ($F(1,19) = 7.06$, $P = 0.0155$), which was significantly faster in fasting than in nonfasting animals (0.0208 ± 0.0039 vs. 0.0102 ± 0.0059 min^{-1}, $P < 0.05$), probably because of faster absorption of ^{18}F-FDG in muscle in the fasting state.

Significant positive correlations were found between ^{18}F-FDG plasma clearance rate and total accumulated radioactivity (at 60 min) in the urinary bladder in intravenous ($R = 0.603$, $P = 0.025$) and intraperitoneal ($R = 0.526$, $P = 0.04$) injection studies. The accumulated radioactivity in the urinary bladder did not correlate with SUV or K_i in the brain, myocardium, or skeletal muscle.

^{18}F-FDG Kinetics in Tissues

Figure 2 and Supplemental Figure 2 show representative ^{18}F-FDG PET images acquired at different times in nonfasting and fasting mice receiving intravenous or intraperitoneal injection. Small-animal PET images were fused with CT images for anatomic reference. The initial transit of the ^{18}F-FDG bolus through the circulatory system was rapid for intravenous injection. Intense radioactivity was seen in the right ventricle within 3 s after injection into the tail vein, followed by a rapid decline. The radioactivity in the right ventricle was already sharply declining when the radioactivity in the left ventricle started to build up and cleared within 2–3 s before the tracer was distributed to different tissues and organs. For intraperitoneal injection, radioactivity was initially intense in the peritoneal cavity, and the tracer was distributed to various organs in approximately 15–20 min after injection. A whole-body distribution profile similar to that obtained with intravenous injection was attained at approximately 25 min after injection. Irrespective of administration route, myocardial ^{18}F-FDG uptake was high in nonfasting mice but low in fasting mice. Throughout the study, ^{18}F-FDG uptake in skeletal muscle was very low, compared with that in the brain and the heart, regardless of administration route and dietary condition. Radioactivity in the urinary bladder was visible on PET images after about 114 and 900 s after intravenous and intraperitoneal injection, respectively.

The time courses of ^{18}F activity in the brain, myocardium, skeletal muscle, liver, left ventricle, renal cortex, and urinary bladder are shown in Supplemental Figure 3. Although tracer uptake was slower for the intraperitoneal route, activity in most tissues and organs reached concentrations comparable to the intravenous route within 60 min after injection. Because of different dietary conditions, the uptake curves differed somewhat. In the brain, SUVs were

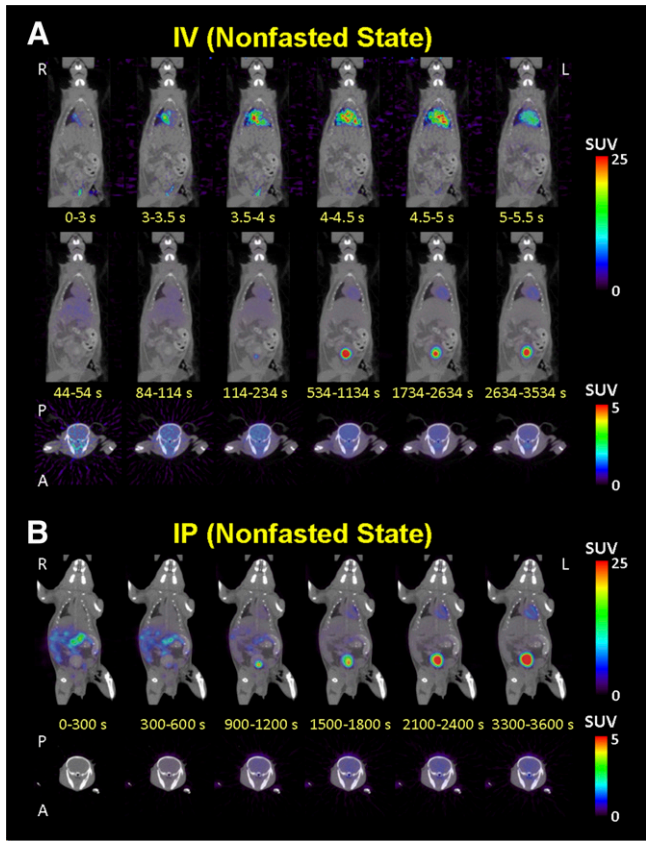

FIGURE 2. Representative examples of biodistribution of ^{18}F-FDG at different times in nonfasting mice after intravenous (A) and intraperitoneal (B) injection. Small-animal PET images are fused with CT images for anatomic localization of structures such as myocardium, lung, liver, gastrointestinal tract, and urinary bladder (shown in coronal view) and brain (shown in transaxial view). Color bars are scaled differently for coronal and transaxial views.

significantly higher in fasting than in nonfasting animals receiving intraperitoneal injection ($P < 0.001$). Myocardial SUVs did not plateau within 60 min in nonfasting animals receiving intraperitoneal injection, unlike the case in nonfasting animals receiving intravenous injection. In the urinary bladder, there was about a 10- to 15-min delay before activity after intraperitoneal injection reached the same level as that after intravenous injection. The elevated activity observed in the left ventricle at late times was likely caused by spillover from the myocardium and was particularly prominent in nonfasting mice.

Tissue ^{18}F-FDG Uptake and Metabolic Parameters

Patlak plots of the brain, myocardium, and skeletal muscle for intravenous and intraperitoneal injection studies are shown in Supplemental Figure 4, which also shows the empiric choices of equilibration time after which the Patlak plot became linear for intravenous ($t^* = 15$ min) and intraperitoneal ($t^* = 30$ min) injection.

Group averages for SUV (45–60 min), K_i, and MRGlu for the brain, myocardium, and skeletal muscle are shown in Figure 3. In the brain, dietary state had a significant effect on SUV ($F(1,19) = 17.61$, $P = 0.0005$) and K_i ($F(1,19) = 10.26$, $P = 0.0047$), both of which were significantly higher in fasting mice receiving intraperitoneal injection ($P < 0.01$), whereas MRGlu did not differ significantly under different dietary conditions and administration routes. In myocardium, dietary condition had a significant effect on SUV ($F(1,19) = 82.76$, $P < 0.0001$), K_i ($F(1,19) = 28.33$, $P < 0.0001$), and MRGlu ($F(1,19) = 32.59$, $P < 0.0001$), all of which were significantly lower in fasting than in nonfasting animals ($P < 0.01$). For skeletal muscle, dietary condition had a significant effect on SUV ($F(1,19) = 8.64$, $P = 0.0084$) and MRGlu ($F(1,19) = 7.13$, $P = 0.015$) but not on K_i ($F(1,19) = 1.92$, $P = 0.18$). There were no significant differences in SUV, K_i, and MRGlu in the brain ($P > 0.32$), myocardium ($P > 0.52$), or skeletal muscle ($P > 0.15$) obtained from intravenous and intraperitoneal injections, indicating that these 2 routes of administration gave results indistinguishable from one another.

Figure 4 illustrates the relationships between arterial blood glucose level and K_i, MRGlu, and SUV in the brain and myocardium. There was a significant inverse relationship between cerebral K_i and blood glucose level (intravenous: $R^2 = 0.598$, $P < 0.01$; intraperitoneal: $R^2 = 0.786$, $P < 0.0001$; pooled data from all studies: $R^2 = 0.711$, $P < 0.0001$). A significant negative correlation was found between brain SUV and blood glucose level for intraperitoneal injection ($R^2 = 0.783$, $P < 0.0001$) and when all animal data were pooled ($R^2 = 0.379$, $P = 0.002$). However, no significant association was found between the cerebral MRGlu and blood glucose level, as shown by the quality of regression lines fitted to intravenous ($R^2 = 0.012$), intraperitoneal ($R^2 = 0.145$), or pooled intravenous and intraperitoneal ($R^2 = 0.018$) data, and the regression slopes were not significantly different from zero. Brain SUV correlated significantly with K_i ($R = 0.510$, $P = 0.013$) but not with MRGlu ($R = 0.128$, $P = 0.56$). Estimates of cerebral MRGlu derived with intravenous and intraperitoneal injection did not differ significantly (23.8 ± 6.4 vs. 22.2 ± 6.8 μmol/100 g/min, $P = 0.74$).

As shown in Figure 4, myocardial K_i did not correlate with blood glucose level (F test, $P > 0.05$), irrespective of administration route and dietary state. Myocardial MRGlu was dependent on blood glucose level modestly in the nonfasting state (F test, $P < 0.05$) but less so in the fasting state (Fig. 4). Myocardial SUV correlated strongly with MRGlu ($R = 0.868$, $P < 0.0001$). Similar results were observed for K_i, SUV, and MRGlu in muscle (Supplemental Fig. 5), although their absolute differences between dietary conditions were less pronounced than in myocardium. Muscle SUV correlated significantly with MRGlu ($R = 0.422$, $P = 0.045$).

DISCUSSION

The present study investigated the impact of dietary condition and blood glucose level on ^{18}F-FDG uptake and kinetic or physiologic parameters in normal tissues and evaluated the feasibility of intraperitoneal injection in small-animal ^{18}F-FDG PET. A few prior studies on rodents used intraperitoneal injection of ^{18}F-FDG for glucose metabolism quantification based primarily on a semiquantitative index such as SUV or percentage injected dose per gram of tissue (*7,20,21*). Our results, based on ^{18}F-FDG biodistribution and uptake, kinetics analysis, and ANOVA, indicate the similarity

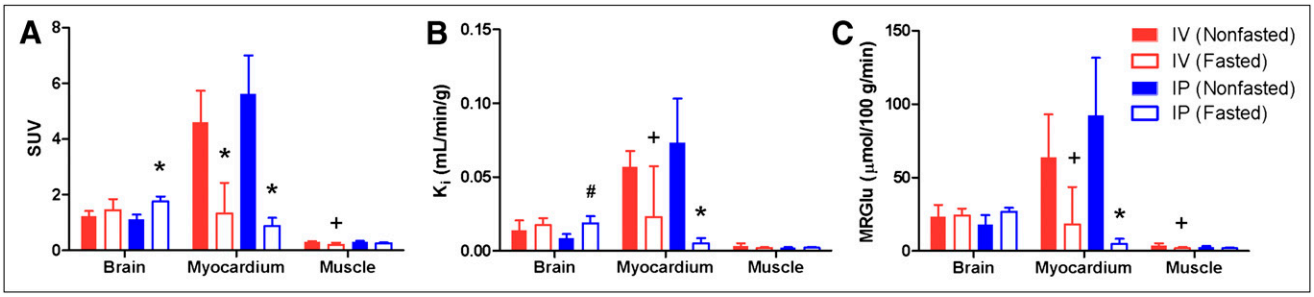

FIGURE 3. Mean SUV (A), K_i (B), and MRGlu (C) of brain, myocardium, and skeletal muscle obtained from nonfasting and fasting animals after intravenous (IV) or intraperitoneal (IP) injection of ^{18}F-FDG. Error bars represent 1 SD. *P* values were calculated using Bonferroni post hoc test ($^{+}P < 0.05$, $^{\#}P < 0.01$, $^{*}P < 0.001$ vs. nonfasting condition using same administration route).

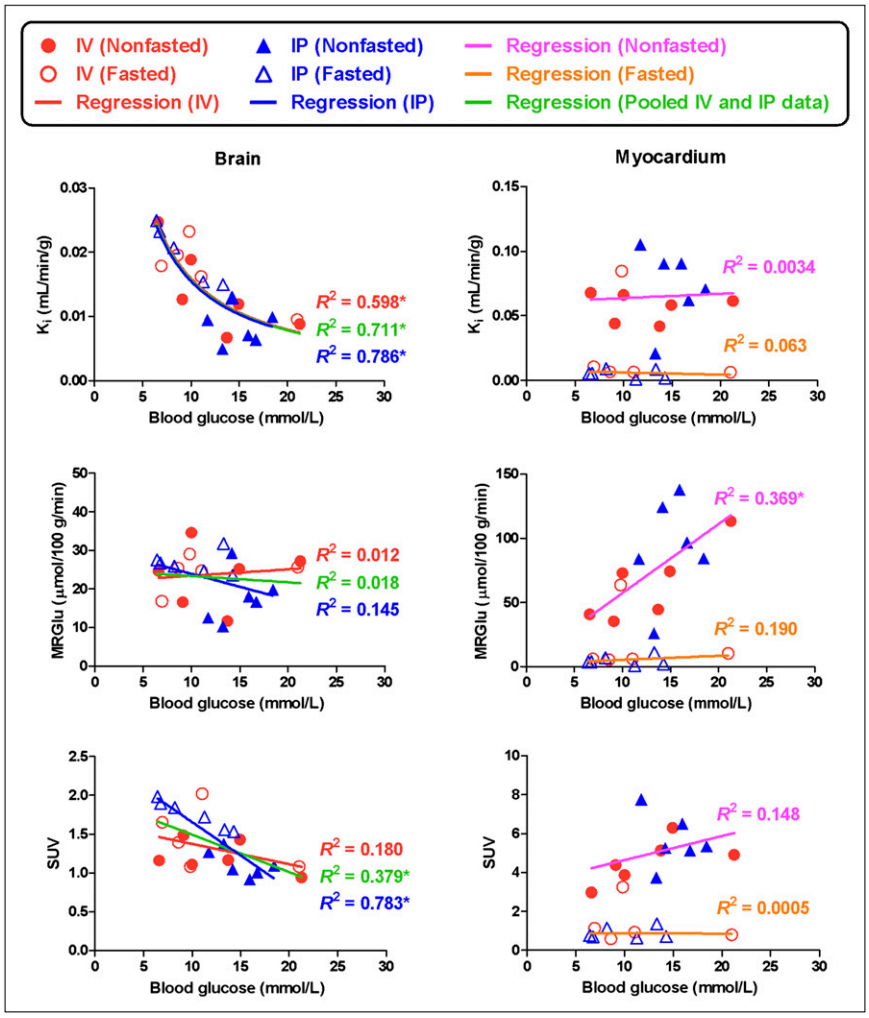

FIGURE 4. Relationships between blood glucose levels and K_i, MRGlu, and SUV in brain and myocardium. *Regression is strongly significant at $P < 0.05$.

between and equivalence of intravenous and intraperitoneal administration routes under different dietary conditions. Although the effect of dietary state on regional ^{18}F-FDG uptake and biodistribution is well known from animal and human studies (*7–13*), to our knowledge no systematic studies have yet been published to elucidate the associations of dietary state and blood glucose level with ^{18}F-FDG K_i and MRGlu in various tissues. Our data show that different mechanisms of glucose utilization exist among the brain, skeletal muscle, and heart muscle, in which K_i and MRGlu were found to be associated differently with blood glucose level and dietary condition.

Effects of Blood Glucose Level and Dietary State on Brain

An inverse relationship was found between cerebral K_i and arterial blood glucose level (Fig. 4). The relationships obtained for intravenous and intraperitoneal data overlap completely, indicating that the derivations of cerebral K_i and MRGlu are independent of administration route. The inverse relationship could not be fully explained by substrate saturation of the glucose transporter, because its half-saturation concentration for glucose is in the range of approximately 6 mmol/L (*22*), which would have caused a reduction in K_i by only one third (instead of one half, based on the observed inverse relationship) when glucose level was doubled from 6 mmol/L. The inverse relationship also implies that cerebral MRGlu stays constant (i.e., independent of blood glucose level) under different dietary states, as is confirmed by the lack of correlation between cerebral MRGlu and blood glucose level (Fig. 4), assuming that the LC does not vary with blood glucose level.

Effects of Blood Glucose Level and Dietary State on Myocardium

Unlike ^{18}F-FDG uptake in the brain, uptake in myocardium varies greatly because cardiac myocytes can derive energy from various competitive substrates, including free fatty acids, glucose, lactate, pyruvate, and ketones, depending on various physiologic and pathologic conditions (*23*). It has long been known that myocardial glucose uptake is diminished by fasting, which is associated with changes in multiple factors, including declined blood glucose and insulin levels and elevated plasma lipid and free fatty acids (*24*). Although insulin level alone would enhance myocardial glucose uptake (*25*), whether the other factors would affect myocardial glucose uptake or transporters was not clear. In

vivo accumulation of ^{18}F-FDG in myocardium has been shown to be much lower in the glucose-loaded (hyperglycemic) state, during which plasma insulin and free fatty acid levels were also remarkably changed (*13*). Our present results show that myocardial K_i is independent of blood glucose level when other factors associated with dietary condition are stable. This finding indicates that the expression of glucose transporters (GLUT4 and GLUT1) (*25*) in the sarcolemma membrane are not responsive to the blood glucose level alone, and the glucose transporters are not saturated within the reference range of glucose level seen in the present study. Because plasma free fatty acid level was not measured in this study, its effect on myocardial glucose transporters will need to be further investigated.

LC

The LC is used to account for differences in transport and phosphorylation rates between ^{18}F-FDG and glucose (*1,2*). In rat brain, the LC was found to be relatively stable within the normoglycemic range (*2*) and decreased slowly in hyperglycemic conditions (*26*). In this study, the blood glucose level measured in most cases is within the standard range observed in mice under general conditions (6.9–14.6 mmol/L (*5*)), except in the nonfasting state, during which the blood glucose level is generally higher. Nonetheless, an LC of 0.6 (*19*), similar to the value (0.625) used by Toyama et al. (*27*) for a similar range of blood glucose level, appears to be reasonable for the calculation of cerebral MRGlu using ^{18}F-FDG PET techniques in mice. In contrast, studies on isolated heart preparations indicated that the LC in myocardium is not well established (*28,29*). Therefore, an LC of unity was used in this study for calculating MRGlu in myocardium and skeletal muscle. The average cerebral MRGlu derived from C57BL/6 mice in this study is in generally good agreement with that derived from isoflurane-anesthetized BALB/c mice (26.0 ± 6.5 μmol/100 g/min, $n = 7$) using ^{18}F-FDG PET and the operational equation of the 2-^{14}C-deoxy-D-glucose method (*27*).

Plasma Clearance

^{18}F-FDG plasma clearance was slightly faster in fasting than in nonfasting mice receiving intravenous injection, and the area under the plasma curve in the fasting state also tended to be slightly lower than that in the nonfasting state. Likewise, ^{18}F-FDG in plasma cleared significantly more quickly in fasting than in nonfasting animals receiving intraperitoneal injection, probably because of higher absorption rates of ^{18}F-FDG in most tissues under the fasting condition. The significant positive correlations between ^{18}F-FDG plasma clearance rate and total accumulated radioactivity in urinary bladder indicated that ^{18}F-FDG plasma clearance is also affected by kidney excretion.

Effects of Anesthesia on Blood Glucose Level

Blood glucose level increased gradually during the imaging experiment. Several studies have indicated that common anesthetic agents induce hyperglycemia and influence the uptake of ^{18}F-FDG in various tissues differently (*7,27,30*). Choice of anesthetic agents, depth of anesthesia, presence of anxiety or stress, and dietary condition are among the confounding variables contributing to the observed increase in blood glucose level and need to be considered when results from anesthetized animals are compared. Nevertheless, the changes in plasma glucose level did not significantly affect the derived physiologic parameters, in which the variations were only minimal, because the slope in the Patlak plot was stable even if the total study duration was shortened (Supplemental Fig. 4).

Quantitation of ^{18}F-FDG Uptake Using SUV

Whether to correct for blood glucose level in the SUV formula has been controversial (*3,4,10*). Our data show that cerebral MRGlu is relatively constant but that, similarly to K_i (Fig. 4), SUV declines with increasing blood glucose level, indicating that correction for blood glucose level is needed in the calculation of SUV to reflect MRGlu. Conversely, SUV in myocardium and skeletal muscle correlates significantly with MRGlu, suggesting that the SUV formula without correction for blood glucose level is a better index of MRGlu. Although SUV has the advantage of simplicity, it is subject to various sources of error and the validity depends on several assumptions and approximations (*3,4*). Even though the variability of SUV appeared to be smaller than that of K_i or MRGlu (Fig. 3), its value may not necessarily reflect MRGlu in the tissue of concern. Therefore, results based on SUV should be interpreted cautiously.

Implications for Tumor Imaging

The present results, although limited to normal tissues, indicate that ^{18}F-FDG uptake mechanisms in the brain, myocardium, and skeletal muscle differ considerably in response to altered blood glucose level and dietary state, suggesting that ^{18}F-FDG uptake and glucose metabolism are controlled differently in different types of cells. This may be true for cancer cells as well. Although limited data obtained in rodents with implanted tumors show that ^{18}F-FDG uptake in tumor remains relatively unchanged with elevated blood glucose level (*12*), results from most in vitro, in vivo, and clinical studies have shown that ^{18}F-FDG uptake in many cancer cells is reduced with increasing blood glucose level (*8–11*), thus indicating that different mechanisms of regulating glucose utilization exist among different tumor cells. Further studies are clearly required to determine the key issues for different tumors.

Advantages and Limitations of Intraperitoneal Injection

Although tail-vein injection is probably the route of first choice for administering radiopharmaceuticals and other drugs to rodents, the procedure is difficult to perform on mice, and partial paravenous injection is common because of the small caliber of the tail vein. Reproducible intravenous injection is not always possible for longitudinal studies (because of damage to the vein) or for sequential or multiple-tracer injection studies (because of residual activity from previous injections). Conversely, intraperitoneal injection appears to be a pragmatic

alternative because it is quick and easy to perform (*6*) and has proved to be reproducible for longitudinal studies (*20*), thereby reducing stress to the animal—a benefit to behavioral studies (*21*) and studies on conscious animals (*31*). Our results indicate that both routes of administration provide equivalent pharmacokinetic parameters and comparable ^{18}F-FDG biodistribution within 60 min after injection. However, initial distribution of intraperitoneally injected ^{18}F-FDG in various organs was slower because ^{18}F-FDG has to diffuse across the peritoneal membrane and the absorption is via the portal system (*32*). Therefore, intraperitoneal injection is not suitable for radiopharmaceuticals or drugs that are eliminated primarily by the liver. In addition, the peritoneal cavity is a space occupied by different abdominal contents. Therefore, there is a risk of incorrectly administering tracer into an organ rather than into the cavity. Reported failure rates for intraperitoneal injection typically range from 10% to 25% (*33*). Nonetheless, according to our experience, failure can be minimized with increasing awareness of potential error, use of an appropriate needle, special care in needle placement, and good training.

CONCLUSION

Our results show that intraperitoneal injection is a valid and practical alternative to the tail-vein injection commonly used in small-animal ^{18}F-FDG PET and provides equivalent pharmacokinetic data. ^{18}F-FDG K_i, SUV, and MRGlu of myocardium and skeletal muscle in mice are strongly dependent on the dietary condition. Myocardial K_i, however, is independent of blood glucose level. In contrast, cerebral K_i varies inversely with blood glucose level. Cerebral MRGlu is not dependent on administration route and does not correlate with blood glucose level or dietary condition. In tissue in which ^{18}F-FDG uptake declines with increasing blood glucose, correction for blood glucose level will make SUV a more robust outcome measure of MRGlu.

DISCLOSURE STATEMENT

The costs of publication of this article were defrayed in part by the payment of page charges. Therefore, and solely to indicate this fact, this article is hereby marked "advertisement" in accordance with 18 USC section 1734.

ACKNOWLEDGMENTS

This work was supported by NIH grants R01-EB001943 and P50-CA086306. We thank Waldemar Ladno, Judy Edwards, Antonia Luu, Benjamin Chun, and David Stout for technical assistance in small-animal PET and CT imaging; the UCLA Cyclotron staff for help with ^{18}F-FDG preparation; and Weber Shao, David Vu, and David Truong for computer and database support.

REFERENCES

1. Huang S-C, Phelps ME, Hoffman EJ, et al. Noninvasive determination of local cerebral metabolic rate of glucose in man. *Am J Physiol.* 1980;238:E69–E82.
2. Sokoloff L, Reivich M, Kennedy C, et al. The [^{14}C]deoxyglucose method for the measurement of local cerebral glucose utilization: theory, procedure and normal values in the conscious and anesthetized albino rat. *J Neurochem.* 1977;28:897–916.
3. Keyes JW Jr. SUV: standard uptake or silly useless value? *J Nucl Med.* 1995; 36:1836–1839.
4. Huang S-C. Anatomy of SUV. *Nucl Med Biol.* 2000;27:643–646.
5. Hubrecht R, Kirkwood J. *The UFAW Handbook on the Care and Management of Laboratory and Other Research Animals*. 8th ed. Oxford, U.K.: Wiley-Blackwell; 2010.
6. Wixson SK, Smiler KL. Anesthesia and analgesia in rodents. In: Kohn DF, Wixson SK, White WJ, Benson GJ, eds. *Anesthesia and Analgesia in Laboratory Animals*. New York, NY: Academic Press; 1997:165–203.
7. Fueger BJ, Czernin J, Hildebrandt I, et al. Impact of animal handling on the results of ^{18}F-FDG PET studies in mice. *J Nucl Med.* 2006;47:999–1006.
8. Wahl RL, Cody RL, Hutchins GD, Mudgett EE. Primary and metastatic breast carcinoma: initial clinical evaluation with PET with the radiolabeled glucose analogue 2-[F-18]-fluoro-2-deoxy-D-glucose. *Radiology.* 1991;179:765–770.
9. Wahl RL, Henry CA, Ethier SP. Serum glucose: effects on tumor and normal tissue accumulation of 2-[F-18]-fluoro-2-deoxy-D-glucose in rodents with mammary carcinoma. *Radiology.* 1992;183:643–647.
10. Lindholm P, Minn H, Leskinen-Kallio S, et al. Influence of the blood glucose concentration on FDG uptake in cancer: a PET study. *J Nucl Med.* 1993;34:1–6.
11. Langen K-J, Braun U, Kops ER, et al. The influence of plasma glucose levels on fluorine-18-fluorodeoxyglucose uptake in bronchial carcinomas. *J Nucl Med.* 1993;34:355–359.
12. Yamada K, Endo S, Fukuda H, et al. Experimental studies on myocardial glucose metabolism of rats with ^{18}F-2-fluoro-2-deoxy-D-glucose. *Eur J Nucl Med.* 1985;10:341–345.
13. Kubota K, Kubota R, Yamada S, et al. Re-evaluation of myocardial FDG uptake in hyperglycemia. *J Nucl Med.* 1996;37:1713–1717.
14. Suckow C, Kuntner C, Chow P, et al. Multimodality rodent imaging chambers for use under barrier conditions with gas anesthesia. *Mol Imaging Biol.* 2009;11:100–106.
15. Chow PL, Rannou FR, Chatziioannou AF. Attenuation correction for small animal PET tomographs. *Phys Med Biol.* 2005;50:1837–1850.
16. Wong K-P, Huang S-C. Modeling approach to estimate [^{18}F]FDG blood sample measurements in mice by use of urinary bladder time-activity data. *IEEE Medical Imaging Conference*. Dresden, Germany; 2008:5572–5576.
17. Ferl GZ, Zhang X, Wu H-M, Huang S-C. Estimation of the ^{18}F-FDG input function in mice by use of dynamic small-animal PET and minimal blood sample data. *J Nucl Med.* 2007;48:2037–2045.
18. Patlak CS, Blasberg RG, Fenstermacher J. Graphical evaluation of blood-to-brain transfer constants from multiple-time uptake data. *J Cereb Blood Flow Metab.* 1983;3:1–7.
19. Ackermann RF, Lear JL. Glycolysis-induced discordance between glucose metabolic rates measured with radiolabeled fluorodeoxyglucose and glucose. *J Cereb Blood Flow Metab.* 1989;9:774–785.
20. Marsteller DA, Barbarich-Marsteller NC, Fowler JS, et al. Reproducibility of intraperitoneal 2-deoxy-2-[^{18}F]-fluoro-D-glucose cerebral uptake in rodents through time. *Nucl Med Biol.* 2006;33:71–79.
21. Schiffer WK, Mirrione MM, Dewey SL. Optimizing experimental protocols for quantitative behavioral imaging with ^{18}F-FDG in rodents. *J Nucl Med.* 2007;48: 277–287.
22. Growdon WA, Bratton TS, Houston MC, et al. Brain glucose metabolism in the intact mouse. *Am J Physiol.* 1971;221:1738–1745.
23. Bing RJ, Fenton JC. Cardiac metabolism. *Annu Rev Med.* 1965;16:1–20.
24. Opie LH, Evans JR, Shipp JC. Effect of fasting on glucose and palmitate metabolism of perfused rat heart. *Am J Physiol.* 1963;205:1203–1208.
25. Kraegen EW, Sowden JA, Halstead MB, et al. Glucose transporters and *in vivo* glucose uptake in skeletal and cardiac muscle: fasting, insulin stimulation and immunoisolation studies of GLUT1 and GLUT4. *Biochem J.* 1993;295:287–293.
26. Schuier F, Oriz F, Suda S, et al. Influence of plasma glucose concentration on lumped constant of the deoxyglucose method: effects of hyperglycemia in the rat. *J Cereb Blood Flow Metab.* 1990;10:765–773.
27. Toyama H, Ichise M, Liow J-S, et al. Absolute quantification of regional cerebral glucose utilization in mice by ^{18}F-FDG small animal PET scanning and 2-^{14}C-DG autoradiography. *J Nucl Med.* 2004;45:1398–1405.
28. Ng CK, Holden JE, DeGrado TR, et al. Sensitivity of myocardial fluorodeoxyglucose lumped constant to glucose and insulin. *Am J Physiol.* 1991;260:H593–H603.
29. Hariharan R, Bray M, Ganim R, et al. Fundamental limitations of [^{18}F]2-deoxy-2-fluoro-D-glucose for assessing myocardial glucose uptake. *Circulation.* 1995; 91:2435–2444.
30. Lee K-H, Ko B-H, Paik J-Y, et al. Effects of anesthetic agents and fasting duration on ^{18}F-FDG biodistribution and insulin levels in tumor-bearing mice. *J Nucl Med.* 2005;46:1531–1536.
31. Mizuma H, Shukuri M, Hayashi T, et al. Establishment of in vivo brain imaging method in conscious mice. *J Nucl Med.* 2010;51:1068–1075.
32. Lukas G, Brindle SD, Greengard P. The route of absorption of intraperitoneally administered compounds. *J Pharmacol Exp Ther.* 1971;178:562–566.
33. Steward JP, Ornellas EP, Beernink KD, Northway WH. Errors in the technique of intraperitoneal injection of mice. *Appl Microbiol.* 1968;16:1418–1419.